

Supplementary Information

Functionalizable poly-terthiophene/Cu₂O heterojunction constructed *in situ* for sensitive photoelectrochemical detection of long non-coding RNA markers

Xuehui Pang^{a*}, Rui Liu^a, Xiaoyi Lv^{a,b}, Wenjun Lu^{a,b}, Lebin Sun^{a,b}, Qiuyan Wang^{a,b},

Zhen Li^d, Qing Kang^d, Jiandong Xie^a, Yingxin Pang^{c*}, Feimeng Zhou^{a*}

^a School of Life Sciences, Tiangong University, Tianjin, P.R. China. E-mail: pxh1118@yeah.net; yingxinpang@126.com; zhoufeimeng@tiangong.edu.cn.

^b College of Chemistry, Chemical Engineering and Materials Science, Shandong Normal University, Jinan, Shandong, P.R. China

^c Department of Obstetrics and Gynecology, Qilu Hospital of Shandong University, Jinan, Shandong, P.R. China

^d Key Laboratory of Interfacial Reaction & Sensing Analysis in Universities of Shandong, School of Chemistry and Chemical Engineering, University of Jinan, Jinan, Shandong, P. R. China

Abbreviations

qRT-PCR—quantitative real-time polymerase chain reaction

ECL—electrochemiluminescence

1. LncRNA Sequences used

1.1. LncRNA TROJAN:

5'-TGT TCA CAC TCA ACT GAC CTT CAG ACT CTC CCT TTC AGG GGA
GAT CTC AT-3'

We blasted the LncRNA TROJAN fragment to ensure that it specifically matches with the triple negative breast cancer.

1.2. Four gene fragments used in the study on selectivity:

5'- ATT TGG AGG ATA ACT CCC AGC TAG AAA GGA AGA AAA GCT CTA
AAG TGG AAT CGC CTT CCC CC GG AAG CTG TTG TAA AA -3'

(L1)

5'- ACT GTT TCT CCG GAC GCT GGA CGC TGC CCG CGT GTT TGG TCT
CTC CGC CG -3'

(ANCR)

5'- TGC CAG CCT CAG CTT AAT CCA GGA GAC AAA GAT TAT TTT CCT
TAT TAT CTC TTC TGC ATA GGA TCT GCA ATC AGA ACT ATT GAA CTT
CTC CAT TCA GAC CGC CAC TCA CAC CTA TGG GAA AAG GGT AAT GTA
TCA TCG GCT TAG CAA CAG GGA -3'

(UCA1)

5'- GTT TCA TGG TAG TGC AGA AGA ATT GAA GCT CAA TAG AAG AAG

(BCRT1)

2. Optimization of sensor performance

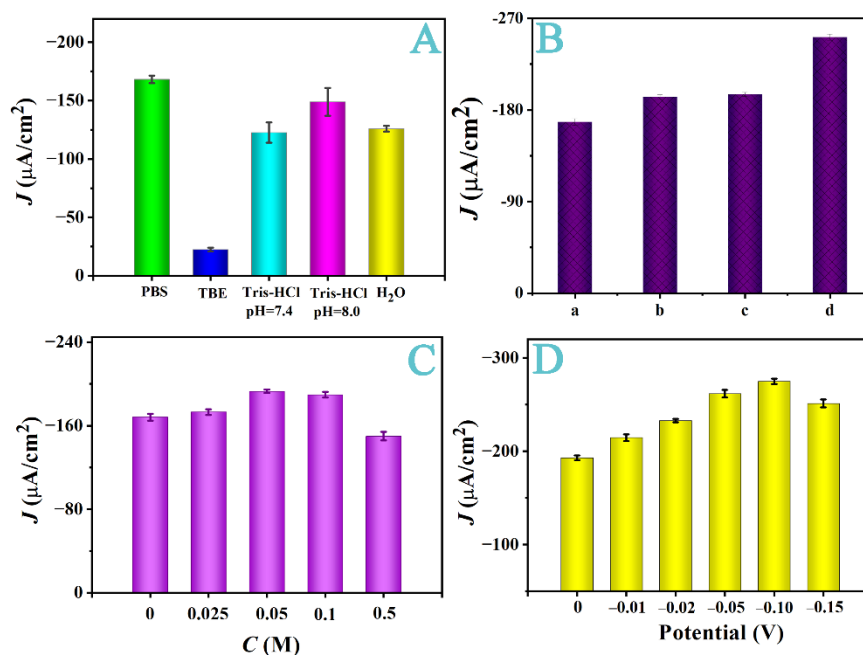


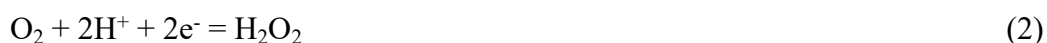
Figure S1. Photocurrent responses at the pTTh/Cu₂O electrode (A) in different electrolyte solutions and (B) in PBS solutions, (a) air-equilibrated without glucose added; (b) air-equilibrated with 0.5 M glucose; (c) deaerated solution without glucose added, and (d) deaerated with 0.5 M glucose. Photocurrent responses (C) in PBS solutions containing different glucose concentrations and (D) in a PBS solution containing 0.05 M glucose at different applied potentials.

In panel A, among the solutions examined, the photocurrent is the highest in PBS. We compared the photocurrent responses in air-equilibrated and deaerated PBS solutions with and without added glucose (panel B). In the air-equilibrated, glucose-containing solution, the current is almost the same as that in the deaerated solution

without glucose. Thus, the addition of glucose obviates the necessity of deaeration. Panel C shows that 0.05 M glucose is optimal for producing the highest photocurrent. Dissolved oxygen in the PBS electrolyte solution acts as an electron acceptor to capture the photoelectrons generated from the photoelectrode material:



The following side reaction generates H_2O_2 , which could react with ascorbic acid or even the electrode materials:¹



When the external voltage is applied to the heterojunction, the current-potential relation can be described by the Shockley equation: $I = I_0[\exp(qV/kT) - 1]$. The applied potential is proportional to the current at a low bias voltage V . However, at a high bias voltage the junction could break down. As shown in panel D, the photocurrent intensity is the largest when the applied external voltage is -0.10 V. However, the electrode surface became partially discolored under an external voltage of -0.15 V, indicating that there is a breakdown of the heterojunction.

Therefore, an external voltage of -0.10 V (vs. Ag/AgCl) was used.

3. Representative functional groups at a MPA-covered pTTh/Cu₂O electrode

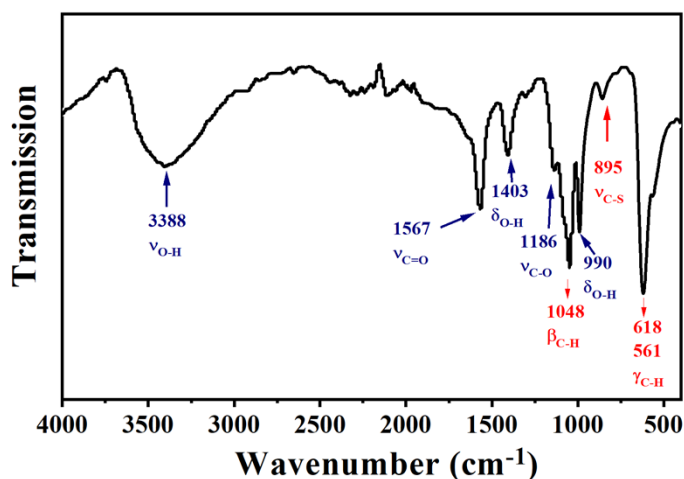


Figure S2. A FT-IR spectrum of a MPA-functionalized pTTh/Cu₂O electrode.

Figure S2 shows broad and scattered stretching vibration peaks in the region of 3600–3000 cm⁻¹. The stretching vibration of C=O ($\nu_{C=O}$) is affected by hydrogen bonding, and $\nu_{C=O}$ shifts to a low wave number at about 1567 cm⁻¹. The ν_{C-O} stretching vibration of carboxylic acid exhibits a prominent peak at approximately 1186 cm⁻¹, while the δ_{O-H} deformation vibration displays two distinct absorption peaks around 1403 cm⁻¹ and about 990 cm⁻¹. These findings confirm that MPA has strongly adsorbed onto the pTTh@Cu₂O heterojunction. Further analysis reveals that the β_{C-H} bending stretching vibration absorption peak on the substituted thiophene ring appears at about 1048 cm⁻¹, and the ν_{C-S} stretching vibration peak² is at about 895 cm⁻¹. The vibration peaks of the middle thiophene ring at about 618 cm⁻¹ and about 562 cm⁻¹ are the γ_{C-H} out-of-plane bending vibration peaks on the 2,5-disubstituted and 2-substituted thiophene rings. In addition, the peak at about 618 cm⁻¹ is sharp and strong, indicating that the polymerization of the triple thiophene mainly occurs at 2 and 5 positions. The torsion angle between the thiophene rings is the

lowest.³ This structure tends to be more planar and the resulting polymer has a high degree of regularity and conjugation.

4. The active surface area measured voltammetrically

The electrochemically active surface area (ECSA) of pTTh/Cu₂O was estimated using the two equations below according to the literature.^{4,5}

$$J_c = \nu C_{dl}$$

where J_c is the double-layer charging current density and C_{dl} represents the double layer capacitance and ν represents the scan rate. The experiment was performed in 0.5 M Na₂SO₄. Voltammograms were collected in a non-Faradaic region at the following scan rates: 0.080, 0.060, 0.040, 0.020, 0.015, and 0.010 V/s. Plotting J_c as a function of ν yields a straight line with slope equal to C_{dl} .

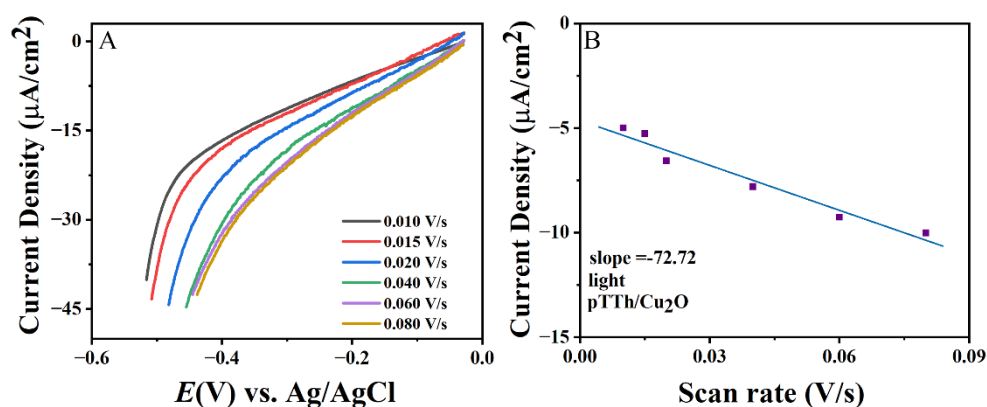


Figure S3. (A) Cyclic voltammograms of pTTh/Cu₂O were collected at different scan rates in a region free of faradaic currents. (B) The cathodic charging currents at 0.16 V were plotted against the scan rate.

The ECSA of pTTh/Cu₂O can be calculated by dividing C_{dl} by the specific

capacitance as shown in the equation below.

$$ECSA = \frac{C_{dl}}{C_s} \quad (2)$$

The ECSA of pTTh/Cu₂O was calculated based on C_{dl} measured and the C_s value from the literature, which are 72.72 $\mu\text{F}/\text{cm}^2$ and 40.00 $\mu\text{F}/\text{cm}^2$,⁶ respectively. Thus, the ECSA is 1.81 cm^2 . The geometric area of our electrode was 1.5 cm^2 . Thus, covering Cu₂O with pTTh has augmented the active surface area of the heterojunction.

5. Mott-Schottky measurements

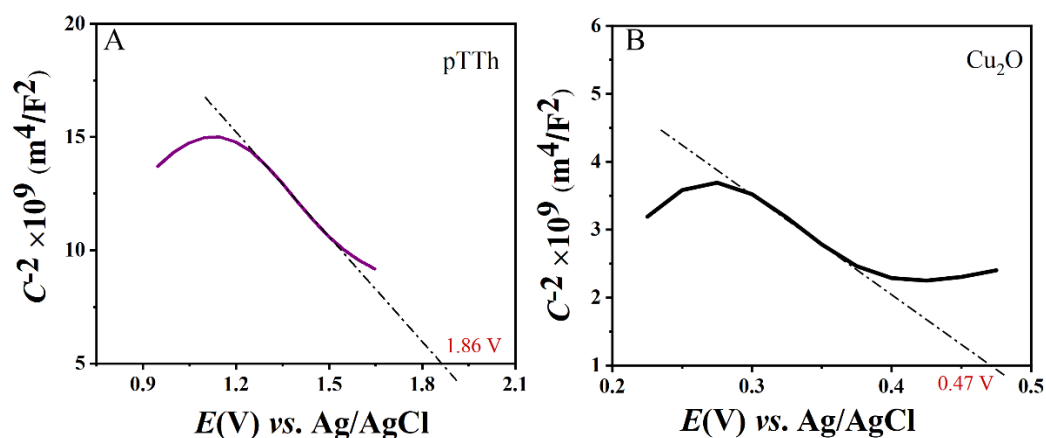


Figure S4. Mott-Schottky plots of (A) Cu₂O and (B) pTTh.

Mott-Schottky (M-S) measurements were conducted in 0.5 M Na₂SO₄ solution at 500 Hz. The relationship between the flat band potential and the semiconductor capacitance is described as follows:

$$\frac{1}{C^2} = \frac{2}{q\epsilon_0\epsilon N_d} \left(V - V_{\text{FB}} - \frac{kT}{q} \right) \quad (3)$$

where C denotes the capacitance at the semiconductor surface, ε the semiconductor's dielectric constant, ε_0 the vacuum permittivity, N_d the carrier density, V the applied potential, V_{FB} the flat band potential, and kT/q the temperature-dependent expression.

The slope is indicative of the type of semiconductor, with positive and negative slopes of straight lines corresponding to n-type and p-type semiconductors, respectively. Both slopes of Cu_2O (-1.48×10^{11}) and pTTh (-1.53×10^9) are negative, confirming that both are p-type semiconductors.^{4,6}

6. Electrochemical impedance spectroscopic (EIS) measurements

Table S1. EIS results of the pTTh/ Cu_2O heterojunction

	Frequency (Hz)	R_t (Ω/cm^2)	C_{dl} ($\mu\text{F}/\text{cm}^2$)
pTTh	10001	2.6	6.12
Cu_2O	1777	10.5	1.51
pTTh/ Cu_2O	1221	50.5	2.58

7. Linear sweep voltammetry

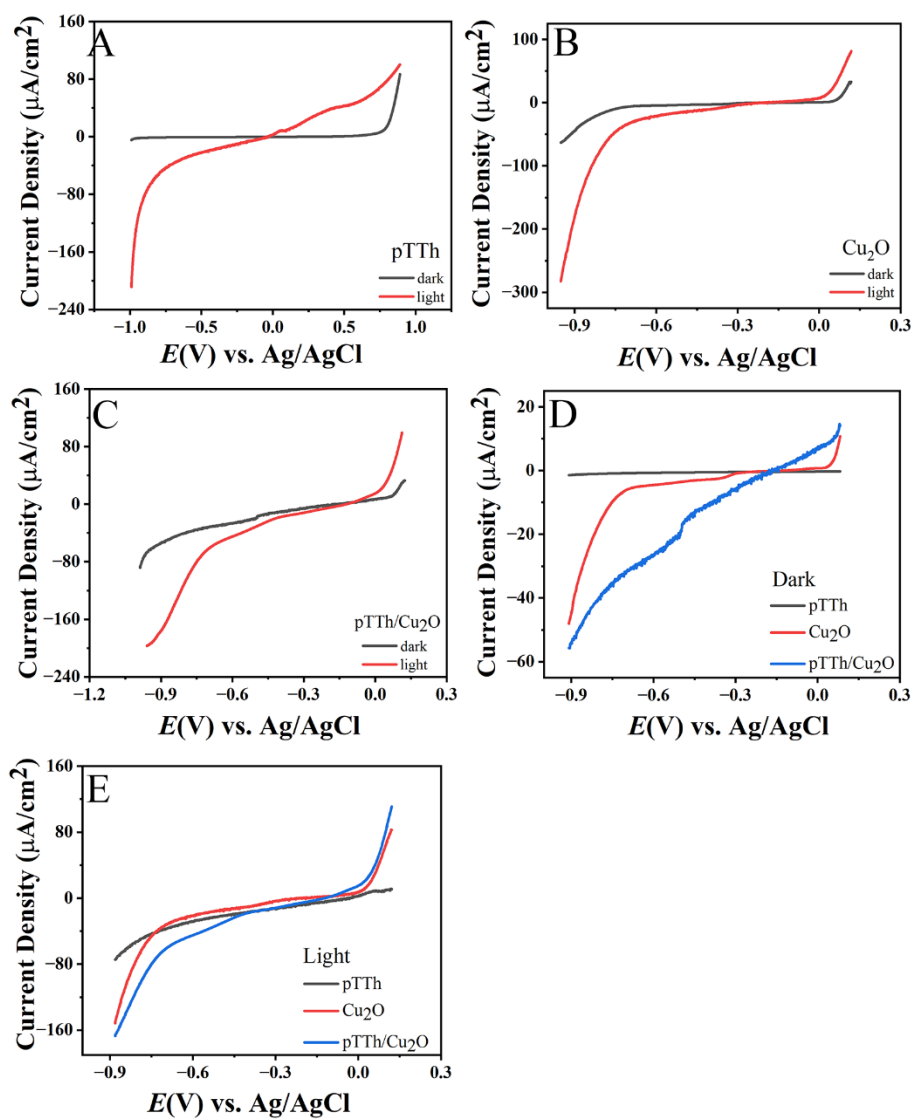


Figure S5. Linear sweep voltammograms of (A) pTTh, (B) Cu_2O , and (C) pTTh/ Cu_2O . Comparisons of the three materials (D) without illumination and (E) with illumination.

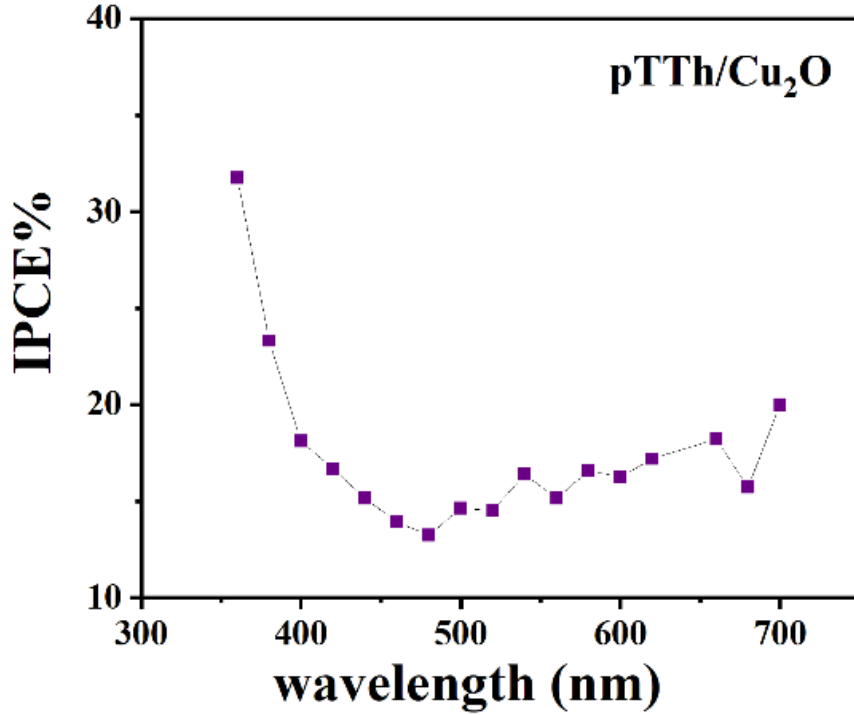


Figure S6. IPCE of pTTh/Cu₂O measured in 0.5 M Na₂SO₄.

8. Incident photon-to-current conversion efficiency (IPCE)

IPCE measurements were conducted at a bias of 0.67 V (Ag/AgCl). The IPCE is defined by the following equation:

$$\text{IPCE} = \frac{1240 \times J}{\lambda P} \times 100\% \quad (4)$$

where λ is the incident light wavelength and P the incident light power density. The IPCE values of pTTh/Cu₂O are greater than 13% (480 nm) across the wavelength range studied. At 360 nm it is even up to 32%, which is higher than those reported by other papers.⁷ Thus, the IPCE is enhanced by the heterojunction.

9. Performance comparisons with other detection methods

10. Electrode functionalization

Table S2. Comparison of different lncRNA detection methods

References	Method	Detection limit	Linear range	Target
this work	PEC	6.64×10^{-14} M	$10^{-8} - 10^{-13}$ M	lncRNA TROJAN
8	Fluorescence	1.7×10^{-15} M	$10^{-14} - 10^{-12}$ M	lncRNA HOTAIR
9	DPV	Not mentioned	$10^{-12} - 10^{-7}$ M	lncRNA HOTAIR
10	qRT-PCR	2.0×10^{-17} M	Not mentioned	lncRN AHOTAIR
		2.0×10^{-17} M	Not mentioned	lncRNA HOTTIP
		5.0×10^{-17} M	Not mentioned	lncRNA H19
11	Fluorescence	3.2×10^{-17} M	$10^{-6} - 10^{-11}$ M	lncRNA MALAT1
12	Fluorescence	8.7×10^{-19} M	$10^{-18} - 10^{-10}$ M	lncRNA MALAT1
13	DPV	4.3×10^{-14} M	$10^{-8} - 10^{-14}$ M	lncRNA MALAT1
14	Fluorescence	6.0×10^{-14} M	$10^{-12} - 10^{-7}$ M	lncRNA HULC
15	Chronopotentiometry	5.0×10^{-15} g/L	$5.0 \times 10^{-15} - 10^{-6}$ g/L	lncRNA HOTTIP
16	qRT-PCR	1.96×10^{-12} g	$10^{-10} - 10^{-7}$ g	lncRNA-ATB

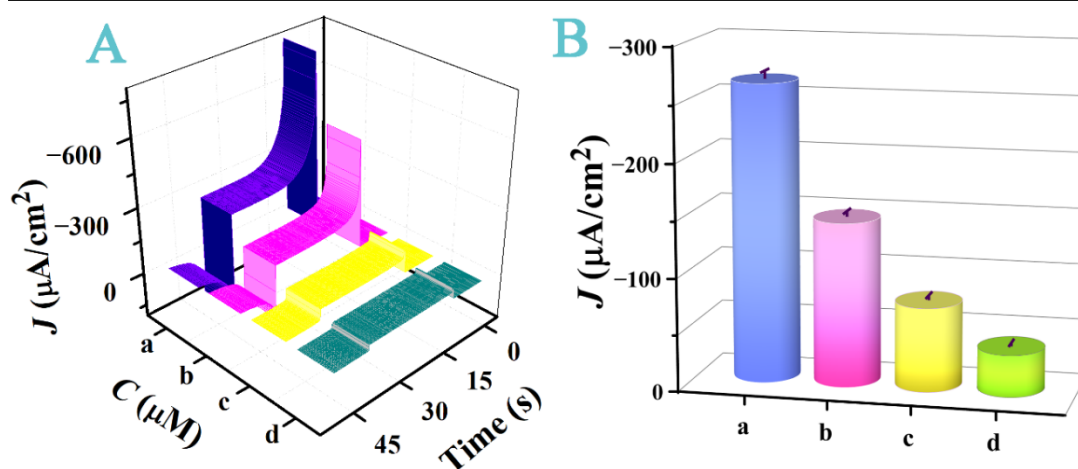


Figure S7. (A) Photocurrent-time responses and (B) steady-state photocurrents at (a) pTTh/Cu₂O, (b) MPA-covered pTTh/Cu₂O, (c) probes immobilized onto the MPA-covered pTTh/Cu₂O and (d) lncRNA TROJAN (10^{-3} $\mu\text{mol}\cdot\text{L}^{-1}$)/probe/MPA-covered pTTh/Cu₂O.

The electrode functionalization process was evaluated. pTTh@Cu₂O/ITO shows a high photocurrent response signal (curve a). The photocurrent at an MPA-

pTTh@Cu₂O/ITO decreases due to adsorption of MPA to pTTh@Cu₂O, likely through hydrogen-bonding (curve b). The probes were affixed on the electrode surface via amide bond formation between the amino groups on the probe and the carboxyl groups of MPA (curve c). The duplex formation between the probe and lncRNA TROJAN leads to a further decrease of the photocurrent (curve d).

References

1. H. R. Molavian, M. Kohandel and S. Sivaloganathan, *Front. Physiol.*, 2016, **7**.
2. Y. Furukawa, M. Akimoto and I. Harada, *Synthetic Met.*, 1987, **18**, 151-156.
3. S. Geetha and D. C. Trivedi, *Synthetic Met.*, 2005, **155**, 232-239.
4. W. Fan, B. Zhang, X. Wang, W. Ma, D. Li, Z. Wang, M. Dupuis, J. Shi, S. Liao and C. Li, *Energy Environ. Sci.*, 2020, **13**, 238-245.
5. C. C. L. McCrory, S. Jung, J. C. Peters and T. F. Jaramillo, *J. Am. Chem. Soc.*, 2013, **135**, 16977-16987.
6. X. Deng, R. Li, S. Wu, L. Wang, J. Hu, J. Ma, W. Jiang, N. Zhang, X. Zheng, C. Gao, L. Wang, Q. Zhang, J. Zhu and Y. Xiong, *J. Am. Chem. Soc.*, 2019, **141**, 10924-10929.
7. Y. Wang, H. Shi, K. Cui and J. Yu, *Appl. Catal. B*, 2019, **250**, 171-180.
8. S. Jiang, Q. Liu, W. J. Liu, L. Cui and C. Y. Zhang, *Sensor. Actuat. B-Chem.*, 2022, **358**, 131521.
9. K. Clack, N. Soda, S. Kasetsirikul, R. Kline, C. Salomon and M. J. A. Shiddiky, *Biosens. Bioelectron.*, 2022, **12**, 287.

-
10. C. J. Yuan, J. Fang and W. L. Fu, *Anal. Chem.*, 2023, **95**, 8291-8298.
 11. Q. Zhang, C. Su, X. R. Tian and C. Y. Zhang, *Anal. Chem.*, 2023, **95**, 8097-8104.
 12. N. Zhao, X. Yu, X. Tian, Q. Xu and C. Zhang, *Anal. Chem.*, 2023, **95**, 3082-3088.
 13. M. Chen, D. Wu, S. Tu, C. Yang, D. Chen and Y. Xu, *Sci. Rep.*, 2021, **11**, 3666.
 14. Y. H. Yao, C. J. Duan, Y. Chen, Z. Q. Hou, W. T. Cheng, D. Y. Li, Z. Y. Wang and Y. Xiang, *Anal. Chem.*, 2023, **95**, 1549-1555.
 15. X. H. Pang, X. Zhang, K. K. Gao, S. Wan, C. Cui, L. Li, H. B. Si, B. Tang and W. H. Tan, *ACS Nano*, 2019, **13**, 1817-1827.
 16. K. Khoothiam, P. Boonbanjong, T. Iempridee, P. Luksirikul and D. Japrungr, *Anal. Biochem.*, 2021, **629**, 114212.